Repurposing of existing FDA approved drugs for Neprilysin inhibition: An *in-silico* study

Runali Sankhe[a], Ekta Rathi[b], Suman Manandhar[a], Avinash Kumar[b], Sreedhara Ranganath K Pai[a], Suvarna G Kini[b], Anoop Kishore[a,*]

[a] *Department of Pharmacology, Manipal College of Pharmaceutical Sciences, Manipal Academy of Higher Education, Manipal – 576104, Karnataka, India*
[b] *Department of Pharmaceutical Chemistry, Manipal College of Pharmaceutical Sciences, Manipal Academy of Higher Education, Manipal – 576104, Karnataka, India*

A B S T R A C T

Neprilysin (NEP) is a neutral endopeptidase with diverse physiological roles in the body. NEP's role in degradation of diverse classes of peptides such as amyloid beta, natriuretic peptide, substance P, angiotensin, endothelins, etc., is associated with pathologies of alzheimer's, kidney and heart diseases, obesity, diabetes and certain malignancies. Hence, the functional inhibition of NEP in the above systems can be a good therapeutic target. In the present study, *in-silico* drug repurposing approach was used to identify NEP inhibitors. Molecular docking was carried out using GLIDE tool. 2934 drugs from the ZINC12 database were screened using high throughput virtual screening (HTVS) followed by standard precision (SP) and extra precision (XP) docking. Based on the XP docking score and ligand interaction, the top 8 hits were subjected to free ligand binding energy calculation, to filter out 4 hits (ZINC000000001427, ZINC000001533877, ZINC000000601283, and ZINC000003831594). Further, induced fit docking-standard precision (IFD-SP) and molecular dynamics (MD) studies were performed. The results obtained from MD studies suggest that ZINC000000601283-NEP and ZINC000003831594-NEP complexes were most stable for 20ns simulation period as compared to ZINC000001533877-NEP and ZINC000000001427-NEP complexes. Interestingly, ZINC000000601283 and ZINC000003831594 showed similarity in binding with the reported NEP inhibitor sacubitrilat. Findings from this study suggest that ZINC000000601283 and ZINC000003831594 may act as NEP inhibitors. In future studies, the role of ZINC000000601283 and ZINC000003831594 in NEP inhibition should be tested in biological systems to evaluate therapeutic effect in NEP associated pathological conditions.

1. Introduction

Neprilysin (NEP) is a neutral endopeptidase. It is also known by different functional names such as common acute lymphoblastic leukemia antigen (CALLA), the cluster of differentiation 10 (CD10), endoprotease 24.11, endopeptidase 24.11 and membrane metalloendopeptidase. NEP is a member of M13 family of zinc peptidase [1]. In the body, NEP cleaves many peptides such as atrial natriuretic peptides, B-type natriuretic peptides, angiotensins (I, II, II, IX), bradykinin, substance P, endothelin I & II, amyloid-β (Aβ), endorphin, neurotensin, vasopressin, etc. [2–4]. The progression of various pathological conditions such as kidney and heart disease [4], obesity [5], diabetes [6,7], few malignancies such as colon cancer, lung cancer and melanomas [8] [9–11], etc. is associated with the peptidase activity of NEP. In 2015, the U.S. Food and Drug Administration (FDA) approved sacubitril/valsartan, the combination of a neprilysin inhibitor and an angiotensin receptor blocker (ARB) respectively, commonly known as angiotensin receptor Neprilysin inhibitor (ARNi), for heart failure with reduced ejection fraction [12]. Further, in 2017, clinical trials involving sacubitril/valsartan treatment groups performed well in the renal failure population as compared to treatment with an ARB (Valsartan) alone [13]. Therefore, NEP has gained considerable attention in the last decade for its peptide degrading property, and its inhibition has therapeutic potential in multiple diseases. But the known and available NEP inhibitors are limited. Hence, drug repurposing using different in-silico tools can aid in speeding up the process of drug discovery for the development of new NEP inhibitors.

The role of NEP has been extensively studied in various diseases. The study report of the PARADIGM trial highlighted the role

of NEP inhibitors in the population of heart failure with reduced ejection fraction [14]. In an *in-vivo* study of subtotal nephrectomy, the renoprotective effect of sacubitril/valsartan was found to be stronger as compared to valsartan alone [15]. According to the result of the U.K. HARP-III trial, the combination of sacubitril/valsartan is effective and is well-tolerated in the chronic kidney disease population [16]. Similarly, various studies are focussed on the importance of NEP on chronic kidney and cardiovascular diseases. NEP inhibition in streptozotocin-induced diabetic mice improved outcomes of cardiac function for heart failure with reduced ejection fraction. In diabetic nephropathy, the combination of the NEP inhibitor thiorphan, with an angiotensin receptor blocker and an angiotensin-converting enzyme II activator showed significant improvement in the condition, by modulating components of the renin-angiotensin system and natriuretic peptide system [6]. The activation of the leptin-aldosterone-neprilysin axis contributes to the pathogenesis of cardiac complications in obese patients [17]. In obesity and type 2 diabetes, NEP inhibition showed improvement in insulin sensitivity and glycaemic control. The inhibition results in modulation of several peptides with glucoregulatory properties such as bradykinin, cholecystokinin, glycogen like peptide, glucose-dependent insulinotropic peptide, secretin, and vasoactive intestinal polypeptide, leading to improved glucose homeostasis and weight loss [18]. A study conducted to evaluate the effect of NEP on nociception concluded that NEP inhibition can be a good strategy for pain management [19]. In cancers such as colon cancer [9,10], lung cancer [11,20], and melanomas [8], the increased levels of NEP is correlated with neoplastic progression. The peptidase activity of NEP and its interaction with Akt/ focal adhesion kinase is assumed to contribute to the pathogenesis of colon cancer [21]. In aggressive melanomas, CD10 (NEP) is the biomarker [8] for detection. A recent report has highlighted the role of ARNi in enhancing anti-inflammatory and natriuretic peptide systems in COVID-19 patients [22,23]. Additionally, the use of ARNi is also recommended for patients suffering from COVID-19 [24]. All these findings highlighted the need for designing novel NEP inhibitors. But, *de novo* drug development is resource intensive and time consuming. Hence, drug discovery by repurposing the existing drugs can be an attractive strategy, with the benefit of reduced developmental risk, especially in the case of NEP inhibitors.

The computation repurposing is known as 'in-silico drug repurposing'. In 2019, in the U.S., approximately 30% of drugs approved was through the drug repurposing approach [25]. The concept of drug repurposing has been already practiced in cardiovascular disorders, cancer, obesity, erectile dysfunction, smoking cessation, stress, psychosis, etc. [26]. Drug repurposing using already approved drugs reduces the time and money on preliminary screening, toxicity studies, clinical trials, bulk manufacturing and formulation development. On the other hand, the establishment of new drug candidates requires lots of time and resources. A good example is the case of allopurinol which was originally approved for cancer and is now available for the treatment of gout [25].

In this context, we decided to identify a series of inhibitors for NEP using *in-silico* drug repurposing. The protein structure of the extracellular domain of NEP with sacubitralat (the active metabolite of sacubitril) was used in the current study. The inhibitor binding pocket in the protein structure of the extracellular domain of human NEP (PDB ID: 5JMY) has already been revealed by Schiering, Nikolaus, et al. [27]. The inhibitor binding pocket contains the catalytically essential triad of HIS583, HIS587 and GLU646. For our drug repurposing study, the structures of 2934 FDA approved drugs were downloaded from the Zinc 12 database. Based on the binding pocket of the NEP inhibitor, the high throughput virtual screening of existing FDA approved drugs was done to find out a new series of NEP inhibitors. To the best of our knowledge, this is the first study based on drug repurposing approach that is being re-

ported and employed for the development of NEP inhibitors using receptor-inhibitor complex.

2. Materials and methods

In the current study, the Maestro Molecular platform (Version 12.1) by Schrodinger, LLC, was used to perform molecular docking and simulation studies on an HP desktop system with Linux Ubuntu 18.04.1 LTS platform, Intel Haswell graphics card, 8GB Ram and Intel core i3-4160 processor.

2.1. Protein preparation and grid generation

X-ray crystallographic structure of the extracellular domain of human NEP (PDB ID: 5JMY) was downloaded from the RCSB protein data bank. The PDB ID: 5JMY has a resolution of 2 Å. Prior to docking and simulation studies, the biological unit of protein was prepared using 'Protein Preparation Wizard' in Schrodinger suite [28]. During the process of protein preparation, the protein was subjected to import and refine, review and modify, and minimize processes. In protein preparation wizard, missing side chains and residues were filled using the Prime tool. The active site and catalytically important residues were retained in the protein structure. The water molecules beyond 5 Å were deleted and stages were generated for hetero atoms. To generate low energy state protein, energy minimization was done using OPLS3e (Optimized potential for liquid stimulation) force field and the prepared protein was used for molecular modelling. To generate a grid around the ligand, the receptor grid generation workflow was used by keeping all functional residues in the grid [29].

2.2. Ligand preparation

The structures of 2934 FDA approved drugs from Zinc 12 database were downloaded [30]. For ligand preparation, the LigPrep tool was employed. The lowest energy 3D structures with correlated chiralities were generated at pH 7.0 ± 2.0 under the OPLS3e force field. In this process, all the ligands were pre-processed, which includes generation of tautomers, ionization state at pH 7.0 ± 2.0 using Epik, addition of hydrogen bond, charged group neutralization, and ligand geometry were optimized [29].

2.3. Ligand docking

All the molecular docking studies were carried out using the ligand docking tool GLIDE (Grid-based Ligand Docking with Energetics) module. The GLIDE module was used for predicting ligand-protein binding modes and ranking. Different scoring functions are involved in GLIDE such as high-throughput Virtual Screening (HTVS), standard precision (SP) and extra precision (XP). First, all the drugs were docked with HTVS mode. But, computationally, HTVS docking does not use descriptor and explicit water technology as used in the XP mode. Hence, to avoid false-positive results, few drugs were reanalyzed using SP and XP modes [31,32].

2.4. Free ligand binding energy calculation

The prime module was used to determine absolute ligand-binding affinities to NEP using MM/GBSA (Molecular mechanics energies generalized Born and surface area continuum Solvation) method. The MM/GBSA assay of top eight XP docked drugs was performed using pose viewer file of GLIDE XP mode. The prime MM/GBSA method is dependent on the VSGB solvation model that uses a variable-dielectric generalized Born model, and water as a solvent under the OPLS3e force field to calculate binding energy [33].

2.5. ADME analysis

For the assessment of the ADME profile, the QikProp tool from the maestro modeling platform was used [33]. The QikProp tool helps in the prediction of the druggable property of best four hits based on ADME analysis. During this process, various descriptors such as molecular weight, cardiotoxicity (QPlogHERG), predicted octanol/water partition coefficient (QPlogPo/w), permeability (QP-PCaco), polar surface area (PSA), % human oral absorption (% Oral Absorption) and Lipinski rule of five were calculated.

2.6. Induced fit docking (IFD)-SP

IFD-SP was carried out using the induced-fit docking module from Maestro molecular modelling platform [34]. Based on the XP GLIDE docking score, binding energy, crucial residues involved and ADME analysis, four (ZINC000000001427, ZINC000001533877, ZINC000000601283, and ZINC000003831594) drugs were selected for IFD–SP docking. In IFD, based on the B-factor, side chains were trimmed with receptor and Van der Waals scaling of 0.70 and 0.50 respectively, and a maximum of 20 poses were set for each ligand. Further, prime side-chain prediction and minimization were performed in which refinement of all residues within 5Å of the ligands' pose and side chains were performed [35]. This process allows the ligand structure and conformation to accommodate nearby reorienting side chains. The ligands and residues were minimized. In induced-fit protein structure, all the ligands were rigorously docked and IFD score for each was calculated using the formula:

IFD Score: $1.0 * \text{Prime\_Energy} + 9.057 * \text{GLIDE Score} + 1.428 * \text{GLIDE\_Ecoul}$

2.7. Molecular dynamics (MD) simulation

The flexibility of the receptor is restricted in grid-based docking systems like XP and IFD. These do not mimic the actual biological systems, where the protein and drug are solvated in water. Hence to tackle this problem, MD simulation was performed. Based on the GLIDE docking score, free binding energy and IFD score, four drugs were selected for MD simulation for 20ns. For MD simulation, three steps were performed, viz., system builder, minimization, and MD simulation. The docked complex of protein and ligand were selected, and the system model was made by predefined SPC solvent under orthorhombic boundary conditions. Next, the system model was subjected to energy minimization until a gradient threshold reached 25 kcal/mol/Å balanced at 300 K temperature and 1 bar pressure via NPT ensemble. In the final step, minimized ligand-protein complex were subjected to MD simulation [36].

2.8. Bioisostere replacement

For optimization of ADME and biological properties of top two selected compounds (ZINC000000601283 and ZINC000003831594), the bioisostere replacement of functional group was performed. The bioisosteric replacement tool from Maestro molecular modelling platform was employed to create bioisosteric structures of better potency and ADME profile. Further, the results of the generated bioisosteres were analysed through interaction of ligands with crucial amino acid residues, XP GLIDE docking score, free binding energy and ADME analysis [37].

3. Results

NEP was prepared at a neutral pH of 7.0 ± 0.2. Two α-helical subdomains were present in the extracellular domain. Both α-helical subdomains of NEP are connected with the linker region

Table 1

Docking score and prime MMGBSA score of top eight drugs.

Sr. No.	Drug	Dock Score (XP)	MMGBSA ∆G bind (Kcal/mol)
1	Sacubitrilat	-15.685	-96.51
2	ZINC000001533877	-14.041	-50.12
3	ZINC000000001427	-12.401	-70.5
4	ZINC000001851195	-11.85	-34.91
5	ZINC000000402909	-9.822	-49.29
6	ZINC000000601283	-9.278	-62.43
7	ZINC000000000797	-8.871	-45.82
8	ZINC000003831594	-8.456	-55.94
9	ZINC000028973441	-8.392	-44.01

and essential catalytic triad are present in the central cavity of both subdomains. In the central cavity, the catalytically important zinc atom is coordinated with the side chains of amino acid residues HIS583, HIS587, and GLU646 [38,27]. In the protein, the co-crystallized ligand, sacubitrilat, is bound to the active site of NEP and showed crucial interactions with HIS583, HIS587 and GLU646 residues. A fourth interaction was provided by the carboxylate oxygen adjacent to the P1 methyl group of sacubitrilat. To generate a receptor grid, receptor grid generation workflow was used and the cubic box of specific dimensions was generated around sacubitrilat to perform molecular docking studies.

3.1. Ligand docking

Around 2934 ligands from Zinc 12 database were screened with HTVS docking mode of GLIDE panel. HTVS docking mode utilizes a small period to a large set of drugs by reducing the final torsional refinement and comprehensive sampling. But, during HTVS docking mode the number of intermediate conformational sampling is limited. Hence, a total of 281 drugs with dock scores less than -5 Kcal/mole were filtered and reanalyzed in SP docking mode. After performing SP docking, around 100 drugs were subjected to an extensive XP docking mode of GLIDE panel. XP docking mode is more accurate, avoids the possibility of false-positive results and gives an appropriate correlation between a good pose of drugs and a good dock score. Finally, based on XP dock score and pivotal interactions, eight active drugs (ZINC000001533877, ZINC000000001427, ZINC000001851195, ZINC000000402909, ZINC000000601283, ZINC000000000797, ZINC000003831594, ZINC000028973441) were identified for further screening. The docking score of co-crystalized ligand sacubitralat was found to be -15.685. All the eight selected drugs showed docking scores between -14.041 to -8.392 (given in Table 1).

All the eight drugs showed similar interaction as sacubitrilat. Schiering, Nikolaus, et al. had reported that the hydrophobic interaction of sacubitrilat with PHE544 was towards the shallow S1 pocket of NEP protein [27]. The charge positive interaction with ARG717 and polar interaction with ASN542 were found to be common in sacubitrilat and selected eight drugs. Even in this study, all the eight drugs showed hydrophobic interactions with PHE544. Sacubitrilat also showed interactions with ASN542, ARG717, ARG110 and ARG102. Our eight selected drugs showed interactions with atleast two of the aforementioned residues. *In-silico* docking studies also showed that all the eight drugs showed interaction with HIS711, which then formed a hydrogen bond with zinc causing the stabilization of zinc transition state [38]. This interaction with zinc and its stabilization might result in decreased catalytic activity of NEP, as it is a zinc dependent endopeptidase.

NEP degrades various peptide substrates at the amino sides of hydrophobic amino acids. According to the reports, the protein structure of NEP consists of a large hydrophobic pocket, containing the side chains ALA543, ILE558, PHE563, MET579, VAL580,

HIS583, VAL692 and TRP693 [39]. The co-crystalized ligand, sacu-bitrilat, showed hydrophobic interaction with ALA543, ILE558, PHE563, MET579, VAL580, VAL692 and TRP693. The eight selected drugs also showed hydrophobic interaction with ALA543, ILE558, PHE563, MET579, VAL580, VAL692 and TRP693. But, the hydrophobic interaction with ILE558, MET579 and TRP693 were missing in interactions of ZINC000000402909, ZINC000003831594 and ZINC000000001427 respectively. Sacubitrilat and the selected eight drugs showed polar, Pi-Pi stacking and cation interaction with HIS583. The interactions with side chains of ALA543, ILE558, PHE563, MET579, VAL580, HIS583, VAL692 and TRP693 may contribute to inhibition of the peptidase activity of NEP. According to previous reports, amino acid residue GLU584 is important for peptidase activity [40] and residues such as ALA543 and ASN542 are important for NEP inhibition [39]. In the current study, all eight selected drugs possess interaction with GLU584, ASN542 and ALA543. The 2D interaction diagrams with a summary of all non-bonding interactions are given in Table 2.

3.2. Free ligand binding energy calculation

The Prime-MMGBSA was employed to calculate the binding energy of the top eight drugs with selected docked poses. All the eight drugs showed stability in the docked pose with ΔG binding energy > -34 Kcal/mol (Described in Table 1). The ΔG binding energy of co-crystallized drug sacubitrilat was found to be -96.51Kcal/mol. The co-crystalized ligand and the eight drugs were found to be stable with docked pose . This finding indicates that the selected drugs may act as NEP inhibitors.

3.3. Induced fit docking (IFD)-SP

After the virtual docking studies, based on the ligand interaction and binding energy of the eight drugs, four ligands showing good values were taken forward for induced fit docking (IFD). In virtual docking protocol, the interactions occur between the binding site of the rigid protein and the flexible ligand. But, this is not the case with the actual ligand-protein interactions in the body, where the target protein undergoes backbone or side-chain movements after binding with ligands. This induces alteration in binding sites of the protein. Also, in the body, the ligand binding site on the proteins conforms to the ligand shape and binding mode. IFD was conducted to resolve the shortcomings of rigid docking protocols. IFD has two main applications; first, it generates the most accurate active complex structure of ligand, which is not possible in virtual molecular docking with rigid protein structure. Second, IFD avoids false-negative results of virtual docking. In virtual docking, screening of the ligands was done with the single conformation of ligands. However, in IFD, 20 confirmers were generated for each ligand. Hence, IFD-SP was carried for ZINC000000001427, ZINC000001533877, ZINC000000601283 and ZINC000003831594, and a maximum of 20 conformers were generated for each ligand based on molecular docking and binding energy. Further, the IFD score and ligand interaction were analyzed for selected drugs. The IFD score and 3D ligand interactions are given in Fig. 1.

ZINC000000001427 showed similar non-bonding interactions as predicted in XP docking. The ZINC000001533877 exhibits a new H-bond interaction with HIS711 with similar non-bonding interactions as observed in XP docking. In ligand interactions of ZINC000000601283, the new H-bond interaction was observed with HIS711 and lost with GLU584. The hydrophobic interaction with ALA543, VAL580, MET579, PHE689, VAL692, TRP693, PHE563 and PHE106 was also lost. Similarly, new hydrophobic interaction was observed with ILE718, and lost with ILE558 and PHE544. The new Pi-Pi stacking interactions were observed with TRP693 and PHE106, and missing with amino acid residue HIS583. The Pi-Pi

cation interaction with ARG717 was retained and lost with ARG110 as predicted in XP docking. ZINC000003831594 retained H-bond interaction with HIS711 and GLU584, showed new H-bond interaction with TRP693, and lost H-bond interaction with ARG717. The new Pi-Pi stacking interaction was observed with PHE106. ZINC000003831594 also showed new hydrophobic interaction with PHE689 and MET579, and hydrophobic interaction missing with TYR545. It also showed similar hydrophobic interaction patterns with other amino acid residues as predicted in XP docking.

3.4. ADME analysis

ADME properties of the four drugs were analyzed using the Quikprop module. The ADME profile was assessed using various descriptor calculations such as molecular weight, QPlogHERG, QPlogPo/w, QPPCaco, % human oral absorption, PSA and Lipinski rule of five (Given in Table 3). All the selected drugs obey the Lipinski rule of five.
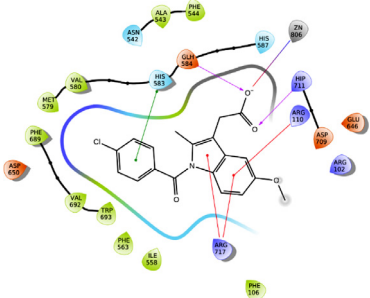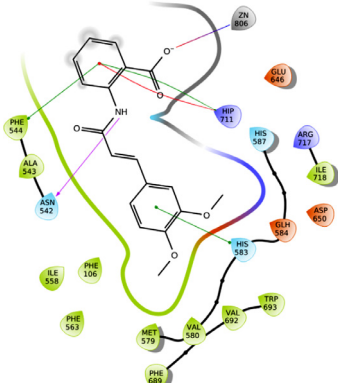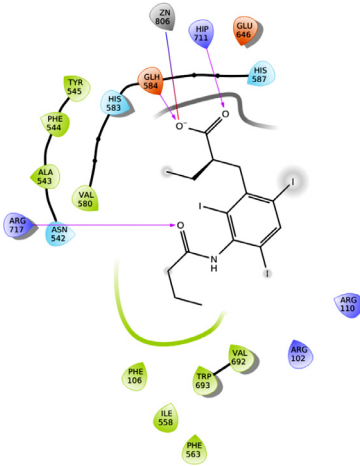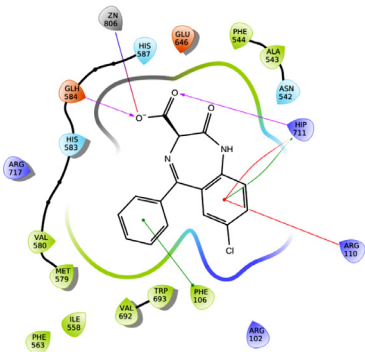
3.5. Molecular dynamics (MD) simulation

Molecular dynamics is used to simulate ligand-protein complexes in presence of systems with biological relevance. It includes the explicit solvent representation with the entire protein. The main advantage of MD stimulation is that it represents the actual conditions of the biological system. It provides a highly dynamic protein structure and the ligand-protein complex is solvated with water, as happens in the biological system [36]. IFD however, provides limited flexibility which is insufficient to mimic the actual conditions of a biological system. Hence, MD simulation studies were carried out to get insights into the top four drugs in terms of binding stability and non-bonding interactions with crucial amino acid within the drug-binding pocket of NEP protein in a dynamic state. In MD simulation, the frame was captured for 20ps which results in the generation of 1000 frames for 20ns stimulation time and saved in a trajectory. Further, RMSD (Root mean square deviation) for NEP protein and 'Lig fit Prot' for the ligands were computed to estimate the stability of ligand-protein complex.

Based on molecular docking score, binding energy and IFD score, the MD simulation was carried out for four ligand-protein complexes viz., ZINC000000001427-NEP docked complex (Complex 1), ZINC000001533877-NEP docked complex (Complex 2), ZINC000000601283-NEP docked complex (Complex 3), and ZINC000003831594-NEP docked complex (Complex 4). For complex 1, RMSD values for protein and ligand were found to be 1.74Å and 1.25Å respectively. The RMSD values were found to be in the acceptable range (1-3Å) but the drift in the ligand-protein complex was observed for a period of 0.5ns-20ns. In case of complex 2, the ligand-protein stabilization was observed from 0-2.2ns and 5-9ns respectively, and drift was observed for 7-20ns. In complex 2, the RMSD values are 1.6Å and 1.2Å for protein and ligand respectively. For complex 3, the RMSD values were found to be 2.2 Å for both. The complex was initially stable, but there was drift for 3-13ns, and eventually stabilization was observed for 13-20ns. According to the results obtained from MD simulation, complex 3 is possibly more stable than complex 1 and 2. Similarly, complex 4 showed RMSD value of 1.9Å for both the protein and the ligand. The complex 4 showed initial drift from 0 to 13ns but eventually stabilized from 13-20ns. Overall, better stability in protein and ligand was observed in complex 3 and 4 compared to complexes 1 and 2. The RMSD plot of selected ligand-protein complexes are given in Fig. 2.

Further, the binding pattern and non-bonding interactions were analyzed for all four complexes. The binding pattern was found to be different for all four complexes. In complex 1, the signifi-

Table 2

2D interaction diagrams of top eight drugs with a summary of all non-bonding interactions.

Sr. No.	Drug	2D ligand interaction diagrams	Non-bonding interaction
1	**Sacubitrilat**		H-bond: GLU584, HIS711, ARG717, ARG102, ASN542 Hydrophobic: MET579, VAL580, ILE558, PHE689, VAL692, TRP693, PHE563, PHE106, ILE718, ALA543, PHE544 Polar: HIS583, HIS587, ASN542 Salt bridge: ZN806, ARG102 Pi-Pi stacking: TRP693, HIS583 Charged Positive: ARG102, HIS711, ARG717, ARG110 Charged Negative: ASP650, GLU646, GLU584
2	**ZINC000001533877**		H-bond: ARG717, GLU584, ALA543, ASN542 Hydrophobic: ILE718, PHE689, VAL692, TRP693, ALA543, PHE544, MET579, VAL580, PHE106, ILE558, PHE563 Polar: THR721, HIS587, HIS583, ASN542 Salt bridge: ZN806, HIS711, ARG110 Pi-Pi Cation: HIS583 Charged Positive: HIS711, ARG717, ARG110 Charged Negative: GLU646, ASP650, GLU584
3	**ZINC000000001427**		H-bond: ALA543, HIS711, GLU584 Hydrophobic: ILE558, PHE544, ALA543, VAL580, MET579, ILE718, PHE689, VAL680, TRP693, PHE563, PHE106 Polar: ASN542, HIS583, HIS587 Salt bridge: ZN806 Pi-Pi Stacking: HIS583, TRP693 Charged Positive: ARG717, HIS711 Charged Negative: ASP650, GLU646
4	**ZINC000001851195**		H-bond: GLU584, HIS711, ALA543, TRP693 Hydrophobic: ILE718, ILE558, ALA543, PHE544, PHE689, ALA690, VAL692, TRP693, MET579, VAL580, PHE563, PHE106 Polar: THR721, HIS587, HIS583, ASN542 Salt bridge: ZN806 Pi-Pi Stacking: TRP693 Charged Positive: ARG717, HIS711, ARG110 Charged Negative: ASP650, GLU646, GLU584
5	**ZINC000000402909**		H-bond: HIS711, GLU584 Hydrophobic: ILE718, ALA543, PHE544, PHE689, VAL692, TRP693, MET579, VAL580, PHE106, PHE563 Polar: HIS587, HIS583, ASN542 Pi-Pi Stacking: PHE106, HIS583 Salt bridge: ZN806 Charged Positive: ARG717, HIS711 Charged Negative: ASP650, GLU646, GLU584

Table 2 (*continued*)

| Sr. No.	Drug	2D ligand interaction diagrams	Non-bonding interaction
6	**ZINC000000601283**		H-bond: HIS711, GLU584 Hydrophobic: PHE544, ALA543, TRP693, VAL692, PHE689, VAL580, MET579, PHE106, ILE558, PHE563 Polar: HIS587, HIS583, ASN542 Salt bridge: ZN806 Pi-Pi Stacking: HIS583 Pi-Pi Cation: ARG717, ARG110 Charged Positive: ARG102, ARG110, HIS711, ARG717 Charged Negative: ASP709, GLU646, GLU584, ASP650
7	**ZINC000000000797**		H-bond: ASN542 Hydrophobic: ILE718, VAL580, MET579, PHE689, VAL692, TRP693, ILE558, ALA543, PHE544, PHE563, PHE106 Polar: HIS587, HIS583, ASN542 Salt bridge: ZN806 Pi-Pi Stacking: HIS711, PHE544, HIS583 Pi-Pi Cation: HIS711 Charged Positive: ARG717, HIS711 Charged Negative: GLU646, GLU584, ASP650
8	**ZINC000003831594**		H-bond: GLU584, HIS711, ARG717 Hydrophobic: VAL580, ALA543, PHE544, TYR545, PHE106, PHE563, ILE558, TRP693, VAL692 Polar: HIS587, HIS583, ASN542 Salt bridge: ZN806 Charged Positive: ARG717, HIS711, ARG110, ARG102 Charged Negative: GLU646, GLU584
9	**ZINC000028973441**		H-bond: GLU584, HIS711 Hydrophobic: MET579, VAL580, PHE544, ALA543, PHE106, TRP693, VAL692, PHE563, ILE558 Polar: HIS587, HIS583, ASN542 Salt bridge: ZN806 Pi-Pi Stacking: PHE106 Pi-Pi Cation: ARG110, HIS711 Charged Positive: ARG717, HIS711, ARG110, ARG102 Charged Negative: GLU646, GLU584, ASP650
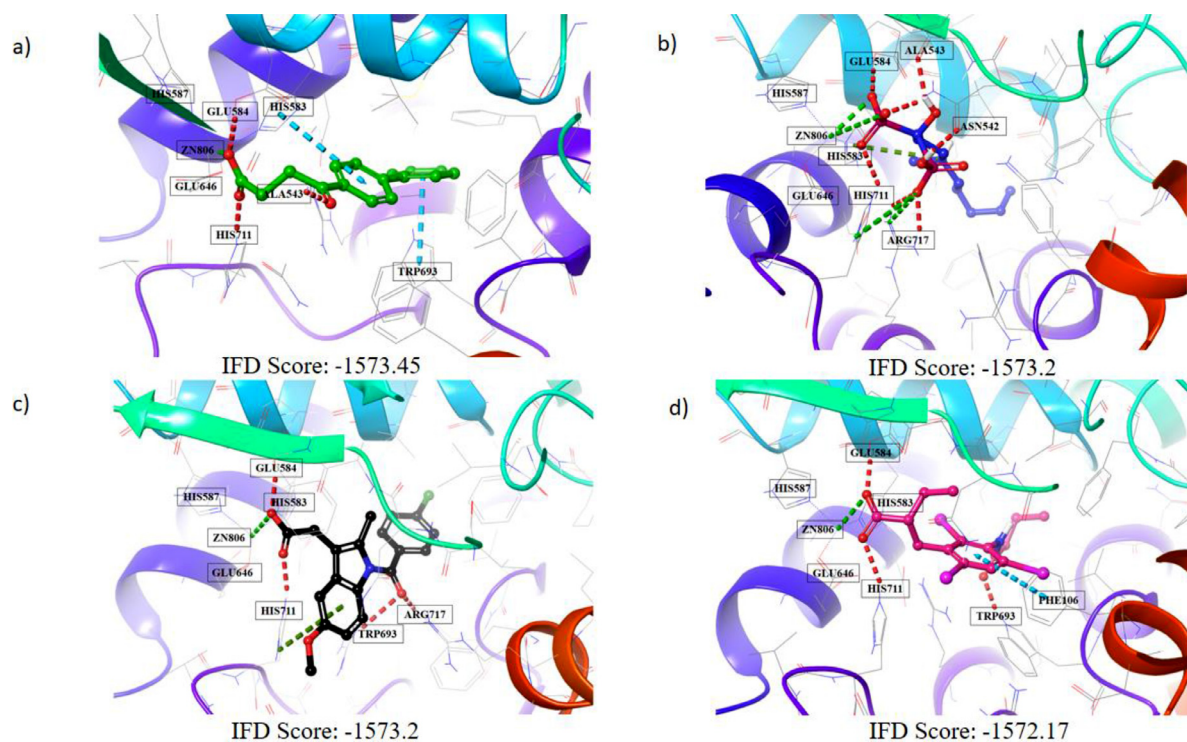
Fig. 1. 3D IFD ligand interactions and scores of the top four selected drugs. Ligand interaction of a) ZINC000000001427 b) ZINC000001533877 c)ZINC000000601283d) ZINC000003831594, with different amino acid residues of NEP.
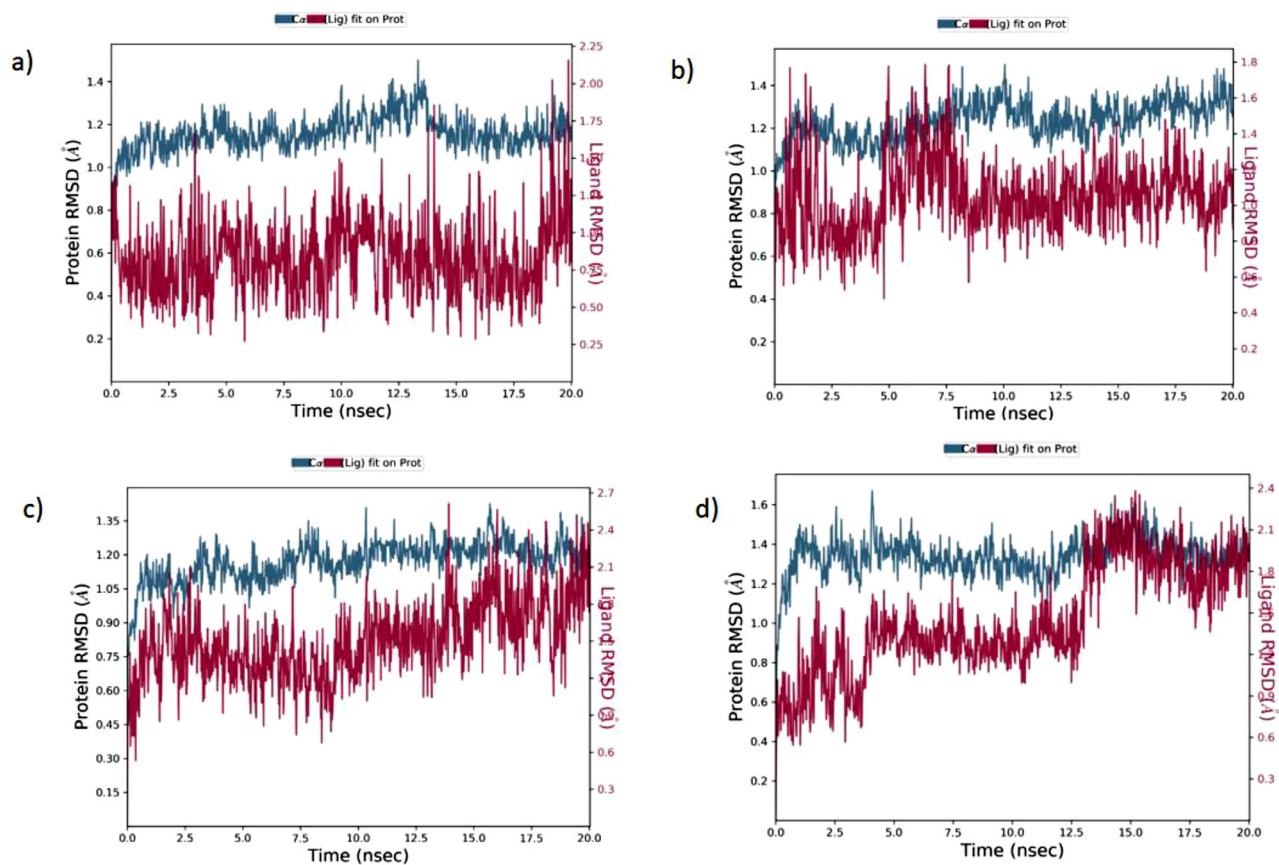

Fig. 2. RMSD plot of ligand-protein complexes. RMSD plot of a) ZINC000000001427 b) ZINC000001533877 c) ZINC000000601283 d) ZINC000003831594, with the active site of NEP.

Table 3
ADME analysis of top four selected drugs using Qikprop.

| Compound Id	Molecular Weight	QPlogP$_{o/w}$	QPlogHERG	QPlogS	QPPCaco	% Oral Absorption	PSA	Rule of five
Sacubitrilat	383.443	3.364	-1.014	-4.031	4.456	58.255	128.646	0
ZINC000001533877	395.432	2.894	-6.747	-3.913	166.560	83.652	92.942	0
ZINC000000001427	254.284	3.198	-3.744	-4.031	97.484	58.255	77.683	0
ZINC000000601283	376.432	2.136	-6.120	-6.120	232.362	81.801	94.166	0
ZINC000003831594	641.026	4.639	-2.581	-2.581	275.682	84.828	76.860	1
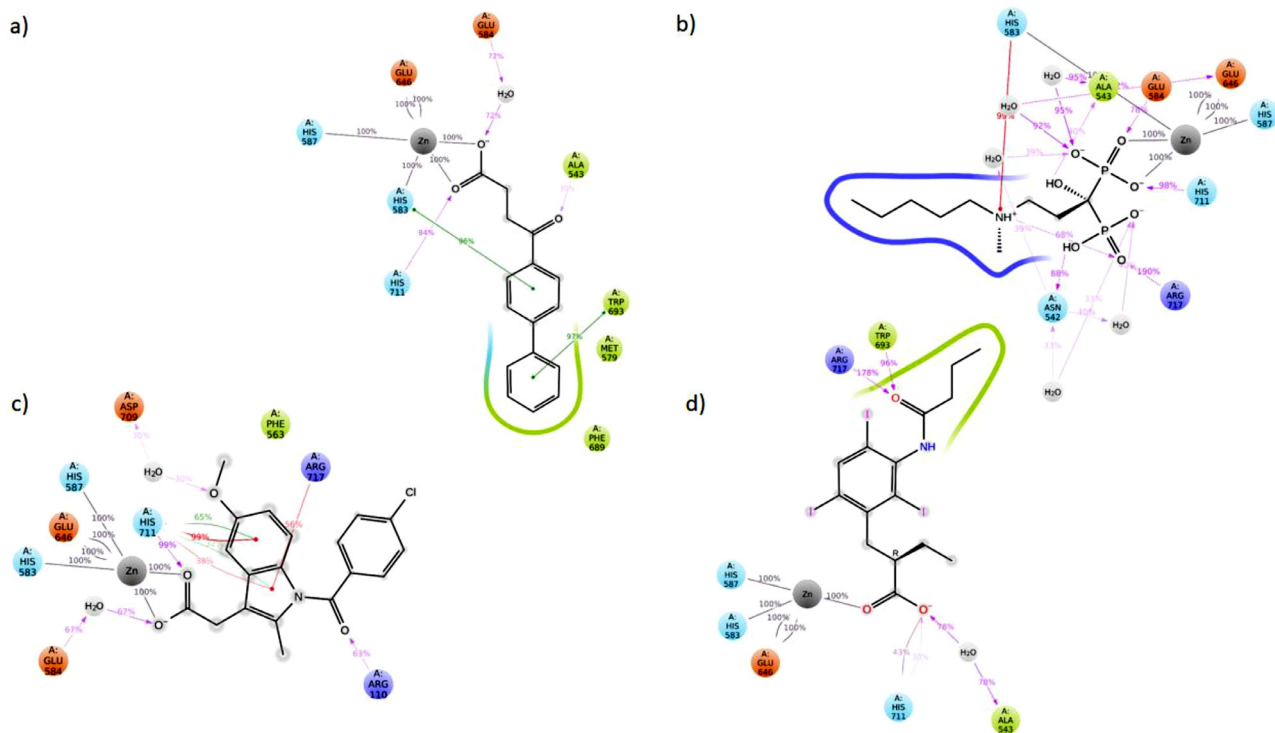
Fig. 3. Ligand-protein interaction diagram obtained after MD stimulation. Ligand interaction of a) ZINC000000001427 b) ZINC000001533877 c) ZINC000000601283 d) ZINC000003831594 with different amino acid residues of NEP.

cant H-bond interactions were observed with amino acid residues GLU584, ALA543 and HIS711, and Pi-Pi interaction with HIS583 and TRP693 as predicted in XP docking. The hydrophobic interactions with ALA543, TRP693, MET579 and PHE689 were retained in MD simulation. On the other hand, hydrophobic interactions with ILE558, PHE544 and PHE563 were missing in MD simulation. The hydrophobic interaction with ALA543, VAL580, ILE718, VAL692 and PHE106 was weaker, affecting the stability of the ligand-protein complex. Similarly, the water bridge-type interaction with GLU584 was observed. In complex 2, strong H-bond interaction was shown by ASN542, ARG717, GLU584 and ALA543. Additional H-bond interactions were also observed with HIS711 and GLU646. The hydrophobic interaction with ALA543, ILE718, PHE689, TRP693, MET579, VAL580, ILE558, PHE106and PHE563 were weakly contributing to the stability of ligand-protein complex, and the interaction was lost with the amino acid residue PHE544. Additional water bridge type of interaction was shown by ASN542, GLU646 and ALA543. The pi-pi cation interactions were retained with HIS583 as predicted in XP docking. In complex 3, H-bond interaction was retained with GLU584 and HIS711, and new H-bond interaction was observed with ASP709 and ARG110. In MD simulation, complex 3 showed weak hydrophobic interaction with ALA543, PHE544, VAL580, TRP693, PHE563, ILE558 and PHE106.The hydrophobic interaction was lost with amino acid residues MET579, PHE689 and VAL692. The new pi-pi stacking interaction was ob-

served with HIS711, however pi-pi stacking interaction was missing with HIS583. The new pi-pi cation interaction was observed with ARG717 and pi-pi cation interaction was missing with ARG110 as compared to XP docking. The additional water bridge type of interaction was shown by ASP709 and GLU584. In complex 4, H-bond interaction was retained with HIS711 and ARG717. New H-bond interactions were found with TRP693 and ALA543 whereas H-bond interaction was lost with GLU584. Complex 4 showed strong hydrophobic interaction with TRP693 and ALA543 whereas weak hydrophobic interaction with VAL680, PHE106, PHE563, ILE558 and VAL692 in contrast to XP docking. Similarly, hydrophobic interaction was missing with amino acid residues PHE544 and TYR545. The additional water bridge type of interaction was observed with ALA543. Among all four complexes, complexes 3 and 4 were found to more stable. The additional H-bond interactions in complexes 3 and 4 may contribute to the stability of the ligand-protein complexes. The ligand-protein MD interaction diagrams and histograms of selected complexes are given Figs. 3 and 4.

3.6. Bioisostere replacement

The ZINC000000601283 (Indomethacin, a non-steroidal anti-inflammatory drug) and ZINC000003831594 (Tyropanoic acid, a radiocontrast agent) were found to be more stable in MD simulation for 20ns. The ZINC000000601283 is anti-inflammatory, anti-pyretic
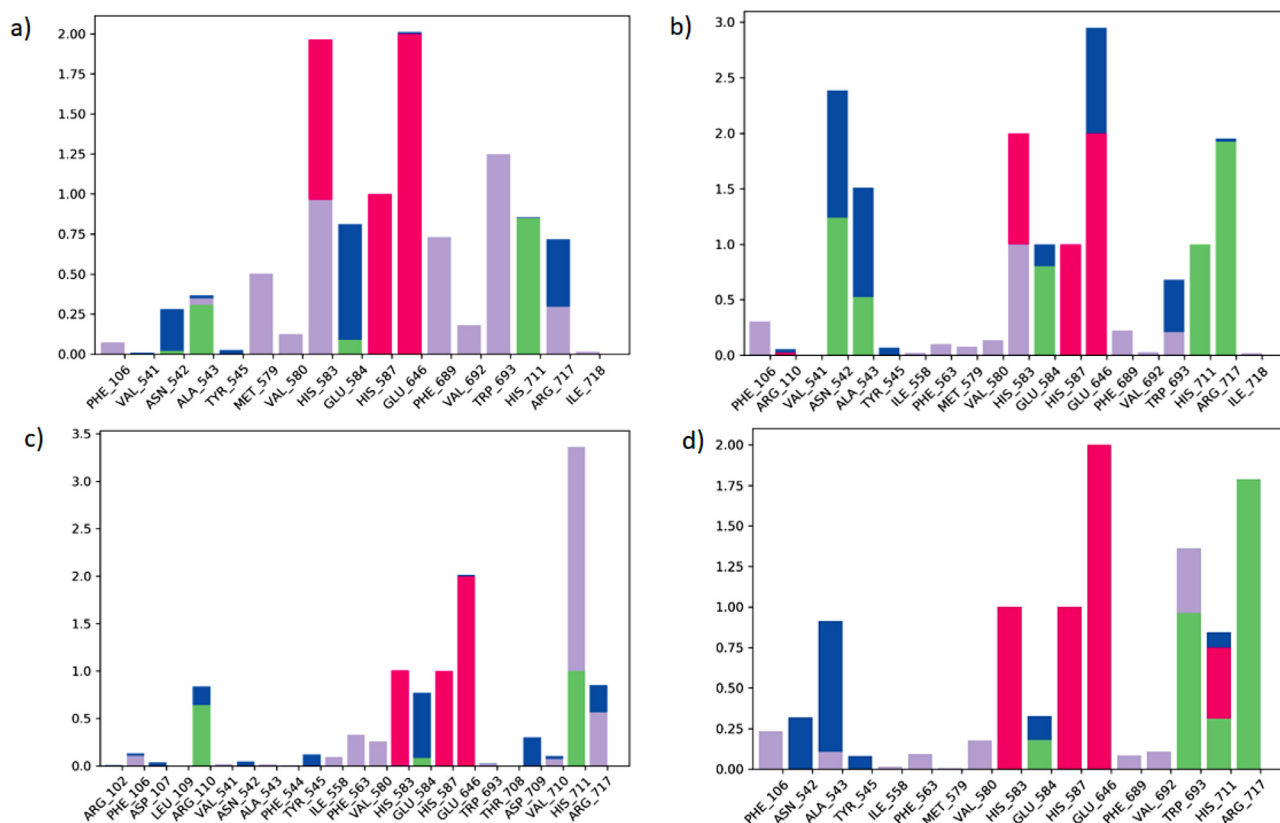
Fig. 4. Histogram of ligand-protein complexes. Histogram of a) ZINC000000001427 b) ZINC000001533877 c) ZINC000000601283 d) ZINC000003831594 with different amino acid residues of NEP.

and analgesic in nature [41]. It is commonly used in rheumatoid arthritis, acute shoulder pains, osteoarthritis, spondylitis and acute gouty arthritis [41]. ZINC000003831594 is known as sodium tyropanoate which is employed in X-ray diagnosis and imaging of gallstones [42]. Though they exhibit good binding affinity for NEP, one of the major disadvantages of ZINC000003831594 is its rapid elimination from the body [41,42]. Therefore, bioisostere replacement of ZINC000000601283 and ZINC000003831594 was performed to enhance biological activity and surpass rapid excretion. Bioisosteres are the molecules which are generated by replacement an atom or a group of atoms from the parent drug with other functional groups [37]. Two main advantages associated with bioisostere replacement are: first, it will result in generation of new bioisostere molecules with similar biological characteristics of the parent drug. Second, bioisosteres can overcome various problems associated with the parent drug's activity, pharmacokinetics and toxicity [37].

During the bioisosteric replacement, 107 and 124 bioisosteric structures of ZINC000000601283 and ZINC000003831594 respectively, were generated. Out of these, the top two bioisosteres were identified based on the ligand interactions with the crucial amino acid residues of NEP, docking score, the binding energy calculated employing MMGBSA, and ADME parameters. The top two selected bioisosteres of ZINC000000601283 and ZINC000003831594 are illustrated by Fig. 5.

The docking scores of the bioisosteres of ZINC000000601283 (structure 1 & structure 2) are 7.125 and -9.103 with binding energies -32.12 and -46.4 Kcal/mol, respectively. Similarly, the docking scores of structure 1 and 2 of ZINC000003831594 were found to be -7.118 and -8.230 with binding energies -53.29 and -55.34

Kcal/mol, respectively (Table 4). Further assessment was done based on the ligand interactions with crucial amino acid residues of the protein compared to the parent drugs (Table 5). Structure 1 of ZINC000000601283 led to the formation of new hydrogen bond interactions with ALA543 and TYR545. Additionally, new π-π cation interactions were observed with HIS711 and ZN806 and hydrophobic interactions with TYR545 and VAL710 by retaining the old interactions. Whereas, structure 2 of ZINC000000601283 had an interaction pattern like similar to the parent drug. However, pi-pi stacking interaction with HIS583 was extinguished. In case of ZINC000003831594, the hydrogen bond interaction of structure 1 and 2 with HIS711 and ARG717 were replaced by salt bridge and π-π cation, respectively. Additionally, HIS583 and ARG110 showed new π-π stacking and cationic interactions and lost the hydrophobic interactions with ILE550 while retaining the other interactions of parent drugs. The bioisosteres of both ZINC000000601283 and ZINC000003831594, showed strong XP-ligand interaction pattern as compared to the parent drugs.

Further, the % oral absorption was observed employing QikProp for parent drugs and bioisostere structures. Here, % oral absorption of the bioisosteres were found to be enhanced in comparison to the parent drugs. The % oral absorption for ZINC000000601283 was 81.801. Whereas, the bioisostere structure 1 and 2 of ZINC000000601283 showed % oral absorption 100 and 88.447, respectively. The parent drug ZINC000003831594 showed % oral absorption 84.828, whereas, the bioisostere structures 1 and 2 of ZINC000003831594 showed % oral absorption 87.382 and 87.565, respectively. The strong ligand interaction and increased % oral absorption of bioisostere structures of both drugs may increase the activity towards NEP as compared to their parent drugs. Therefore,
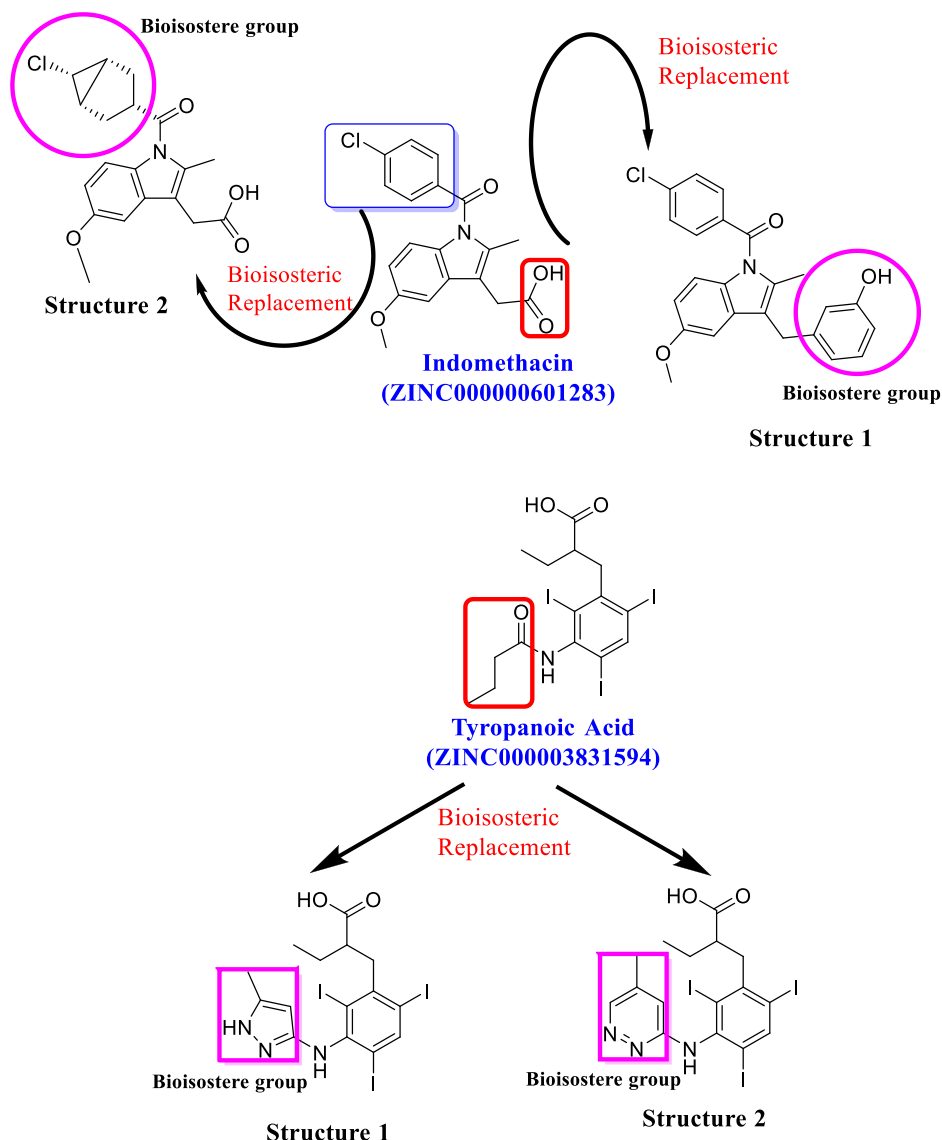
Fig. 5. Bioisosteric replacement of ZINC000000601283 (Indomethacin) and ZINC000003831594 (Tyropanoic acid).

Table 4
Docking score and prime MMGBSA score of bioisosteric structures of ZINC000000601283 and ZINC000003831594.

Sr. No.	Drug	Dock Score (XP)	MMGBSA ΔG bind (Kcal/mol)
A)	**ZINC000000601283**		
1	**Structure 1**	-7.125	-32.12
2	**Structure 2**	-9.103	-46.41
B)	**ZINC000003831594**		
1	**Structure 1**	-7.118	-53.29
2	**Structure 2**	-8.230	-55.34

the designed compounds could be further evaluated for NEP activity as they have shown preferable ADME profile in comparison to parent drugs. The other ADME parameters of bioisostere structure 1 and 2 of ZINC000000601283 and ZINC000003831594 are given in Table 6.

Also, the SwissADME free web server tool [43] was used to determine the metabolism and excretion pattern of ZINC000003831594 and its bioisostere structures. After oral administration, ZINC000003831594 is readily absorbed from small intestine. 2hr after oral administration, it is rapidly excreted into bile which may limit its potential in targeting NEP. The metabolism of the drug is mediated by CYP3A4, CTP2D6 and CYP2C19 enzymes. However, both bioisosteric structures of ZINC000003831594 are inhibitors of CYP3A4 enzyme and their metabolism occurs by CYP1A2, CYP2C19, CYP2C9 and CYP2D6. This observation assumes importance, since CYP3A4 metabolises more than 50% of drugs and endogenous compounds and their biliary excretion [44–46]. Hence, both the bioisosteres of ZINC000003831594 may overcome

Table 5
2D interaction diagrams of bioisosteric structures of ZINC000000601283 and ZINC000003831594 with a summary of all non-bonding interactions.
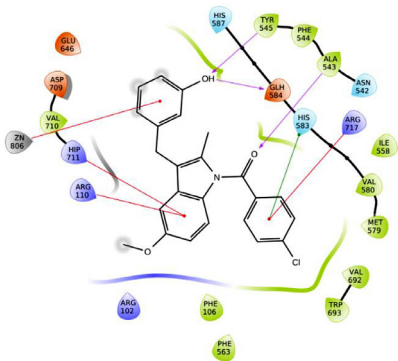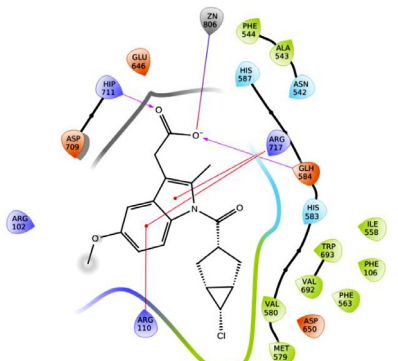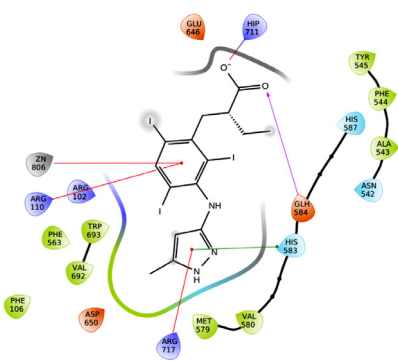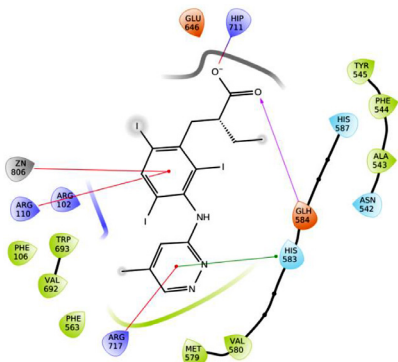
Sr. No.	Drug	2D ligand interaction diagram	Non-bonding interaction
A)	**ZINC000000601283**		
1	**Structure 1**		H-bond: TYR545, GLU584, ALA43 Hydrophobic: TYR545, PHE544, ALA543, ILE558, VAL580, MET579, VAL692, TRP693, PHE563, PHE106, VAL710 Polar: ASN542, HIS583, HIS587, Pi-Pi Stacking: HIS583 Pi-Pi Cation: HIS711, ARG110, ARG717, ZN806 Charged Positive: ARG102, ARG110, ARG717, HIS711 Charged Negative: GLU584, GLU646, ASP709
2	**Structure 2**		H-bond: GLU584, HIS711 Hydrophobic: PHE544, ALA543, ILE558, PHE106, PHE563, TRP693, VAL692, VAL580, MET579 Polar: ASN542, HIS583, HIS587 Salt bridge: ZN806 Pi-Pi Cation: ARG110, ARG717 Charged Positive: HIS711, ARG102, ARG110, ARG717 Charged Negative: GLU646, GLU584, ASP709, ASP650
B)	**ZINC000003831594**		
1	**Structure 1**		H-bond: GLU584 Hydrophobic: TYR545, PHE544, ALA543, VAL580, MET579, TRP693, VAL692, PHE563, PHE106 Polar: ASN542, HIS583, HIS587 Salt bridge: HIS711 Pi-Pi Stacking: HIS583 Pi-Pi Cation: ARG110, ARG717, ZN806 Charged Positive: HIS711, ARG102, ARG110, ARG717 Charged Negative: GLU646, ASP650, GLU584,
2	**Structure 2**		H-bond: GLU584 Hydrophobic: TYR545, PHE544, ALA543, VAL580, MET579, PHE563, VAL692, TRP693, PHE106 Polar: ASN542, HIS583, HIS587 Salt bridge: HIS711 Pi-Pi Stacking: HIS583 Pi-Pi Cation: ARG110, ARG717, ZN806 Charged Positive: ARG102, ARG110, ARG717, ZN806 Charged Negative: GLU646, ASP650, GLU584

Table 6
ADME analysis of bioisosteric structures of ZINC000000601283 and ZINC000003831594 using Qikprop.

Compound Id	Molecular Weight	QPlogPo/w	QPlogHERG	QlogS	QPPCaco	% Oral Absorption	PSA	Rule of five
A) ZINC000000601283								
Structure 1	405.880	5.163	-6.438	-6.438	1441.636	100	56.508	1
Structure 2	361.824	3.601	-2.521	-4.584	181.178	88.447	82.440	0
B) ZINC000003831594								
Structure 1	652.024	4.940	-2.870	-5.693	305.228	87.382	80.407	1
Structure 2	663.035	4.864	-3.023	-5.714	330.847	87.565	78.066	1

the problem associated with the rapid excretion of the parent drug, due to their ability to inhibit CYP3A4 enzyme. Inhibition of metabolism may further prolong their biological activity.

4. Conclusion

In the present study, the *in-silico* drug repurposing approach was used to identify FDA approved drugs for NEP inhibition using the ZINC 12 database. 2934 FDA approved drugs were retrieved from the ZINC 12 database. Initially, all the drugs were subjected to HTVS, SP, and XP docking. Based on docking score and ligand interaction with important amino acid residues, eight drugs (ZINC000001533877, ZINC000000001427, ZINC000001851195, ZINC000000402909, ZINC000000601283, ZINC000000000797, ZINC000003831594 and ZINC000028973441) were identified as hits. All the eight drugs showed non-bonding interactions with residues involved in active site on NEP (HIS583, HIS587 and GLU646) and the hydrophobic pocket of NEP (ALA543, ILE558, PHE563, MET579, VAL580, HIS583, VAL692 and TRP693) which was important for peptidase activity. Further, the binding energy of the top eight selected drug was calculated. All the eight drugs showed significant ΔG binding energy $>$ -34 Kcal/mol. Based on ΔG binding energy, the top four hits were screened for ADME analysis. All four selected drugs showed acceptable ADME profile in terms of molecular weight, QPlogPo/w, QPPCaco, % human oral absorption, PSA, and Lipinski's rule of five when compared with the standard drug sacubitrilat. The QPlogHERG was estimated as -1.014 for sacubitrilat whereas -4.031, -6.747, -6.120 and -2.581 for ZINC000000001427, ZINC000001533877, ZINC000000601283 and ZINC000003831594, respectively. The ADME analyses indicate that, the selected four drugs might be less cardiotoxic compared to sacubitrilat, with a lesser tendency to block HERG K^+ channel. Further, the IFD-SP analysis was done for the top four selected drugs. Based on the binding pattern, ligand interaction and IFD-SP score, the best conformer was selected for each of the four selected drugs and opted for MD simulation. In MD simulation, all ligand-protein complexes showed acceptable RMSD values. But significant ligand-protein stability was observed in complexes 3 and 4 as compared to complexes 1 and 2. Further the bioisosteres replacement approach was used to enhance the biological activity ZINC000000601283 and ZINC000003831594 against NEP.

Based on the results obtained from the present study, ZINC000000601283 and ZINC000003831594 showed interactions similar to sacubitrilat, with desirable ADME profiles. Hence ZINC000000601283 and ZINC000003831594 and their bioisosteric structures might act as potential inhibitors of NEP. However, further *in-vitro* and *in-vivo* studies using models of NEP inhibition need to be conducted to confirm the *in-silico* predictions.

Author statement

Sr No.	Author	Contribution
1.	Runali Sankhe	Conceptualization, in-silico modeling, analysis and interpretation of data, andoriginal draft preparation,
2.	Ekta Rathi	in-silico modeling, interpretation of data, data curation and editing
3.	Suman Manandhar	Data curation and reviewing
4.	Avinash Kumar	in silico modeling
5.	K. Sreedhara Ranganath Pai	Reviewing
6.	Suvarna G Kini	Reviewing
7.	Anoop Kishore	Supervision, reviewing and editing

Declaration of Competing Interest

None

Acknowledgment

References

[1] A. Bayes-Genis, J. Barallat, A.M. Richards, A test in context: neprilysin: function, inhibition, and biomarker, J. Am. Coll. Cardiol. 68 (6) (2016) 639–653, doi:10.1016/j.jacc.2016.04.060.

[2] R. Sankhe, M. Kinra, J. Mudgal, D. Arora, M. Nampoothiri, Neprilysin, the kidney brush border neutral proteinase: a possible potential target for ischemic renal injury, Toxicol. Mech. Methods 30 (2) (2020) 88–99, doi:10.1080/15376516.2019.1669246.

[3] N. Nalivaeva, N. Belyaev, I. Zhuravin, A. Turner, The Alzheimer's amyloid-degrading peptidase, neprilysin: can we control it? Int. J. Alzheimer's Dis. 2012 (2012), doi:10.1155/2012/383796.

[4] V. Malek, A.B. Gaikwad, Neprilysin inhibitors: a new hope to halt the diabetic cardiovascular and renal complications? Biomed. Pharmacother. 90 (2017) 752–759, doi:10.1016/j.biopha.2017.04.024.

[5] K.F. Standeven, K. Hess, A.M. Carter, G.I. Rice, P.A. Cordell, A.J. Balmforth, B. Lu, D.J. Scott, A.J. Turner, N.M. Hooper, Neprilysin, obesity and the metabolic syndrome, Int. J. Obes. 35 (8) (2011) 1031, doi:10.1038/ijo.2010.227.

[6] V. Malek, N. Sharma, H. Sankrityayan, A.B. Gaikwad, Concurrent neprilysin inhibition and renin-angiotensin system modulations prevented diabetic nephropathy, Life Sci. 221 (2019) 159–167, doi:10.1016/j.lfs.2019.02.027.

[7] J.P. Seferovic, B. Claggett, S.B. Seidelmann, E.W. Seely, M. Packer, M.R. Zile, J.L. Rouleau, K. Swedberg, M. Lefkowitz, V.C. Shi, Effect of sacubitril/valsartan versus enalapril on glycaemic control in patients with heart failure and diabetes: a post-hoc analysis from the PARADIGM-HF trial, The Lancet Diabetes & Endocrinol. 5 (5) (2017) 333–340, doi:10.1016/S2213-8587(17)30087-6.

[8] M. Thomas-Pfaab, J.-P. Annereau, C. Munsch, N. Guilbaud, I. Garrido, C. Paul, P. Brousset, L. Lamant, N. Meyer, CD10 expression by melanoma cells is associated with aggressive behavior in vitro and predicts rapid metastatic progression in humans, J. Dermatol. Sci. 69 (2) (2013) 105–113, doi:10.1016/j.jdermsci.2012.11.003.

[9] H. Kuniyasu, Y. Luo, K. Fujii, T. Sasahira, Y. Moriwaka, N. Tatsumoto, T. Sasaki, Y. Yamashita, H. Ohmori, CD10 enhances metastasis of colorectal cancer by abrogating the anti-tumoural effect of methionine-enkephalin in the liver, Gut 59 (3) (2010) 348–356, doi:10.1136/gut.2009.178376.

[10] M. Mizerska-Kowalska, A. Bojarska-Junak, J. Jakubowicz-Gil, M. Kandefer-Szerszeń, Neutral endopeptidase (NEP) is differentially involved in biological activities and cell signaling of colon cancer cell lines derived from various stages of tumor development, Tumor Biol. 37 (10) (2016) 13355–13368, doi:10.1007/s13277-016-5248-y.

[11] K. Leithner, C. Wohlkoenig, E. Stacher, J. Lindenmann, N.A. Hofmann, B. Gallé, C. Guelly, F. Quehenberger, P. Stiegler, F.-M. Smolle-Jüttner, Hypoxia increases membrane metallo-endopeptidase expression in a novel lung cancer ex vivo model–role of tumor stroma cells, BMC Cancer 14 (1) (2014) 40, doi:10.1186/1471-2407-14-40.

[12] L. Fala, Entresto (Sacubitril/Valsartan): first-in-class angiotensin receptor neprilysin inhibitor FDA approved for patients with heart failure, Am. Health Drug Benefits 8 (6) (2015) 330.

[13] R. Haynes, D. Zhu, P.K. Judge, W.G. Herrington, P.A. Kalra, C. Baigent, Chronic kidney disease, heart failure and neprilysin inhibition, Nephrol. Dialysis Transpl. (2019), doi:10.1093/ndt/gfz058.

[14] A.A. Voors, M. Gori, L.C. Liu, B. Claggett, M.R. Zile, B. Pieske, J.J. McMurray, M. Packer, V. Shi, M.P. Lefkowitz, Renal effects of the angiotensin receptor neprilysin inhibitor LCZ696 in patients with heart failure and preserved ejection fraction, Eur. J. Heart Fail. 17 (5) (2015) 510–517, doi:10.1002/ejhf.232.

[15] K. Ushijima, H. Ando, Y. Arakawa, K. Aizawa, C. Suzuki, K. Shimada, S.i. Tsuruoka, A. Fujimura, Prevention against renal damage in rats with subtotal nephrectomy by sacubitril/valsartan (LCZ696), a dual-acting angiotensin receptor-neprilysin inhibitor, Pharmacol. Res. Persp. 5 (4) (2017), doi:10.1002/prp2.336.

[16] Randomized multicentre pilot study of sacubitril/valsartan versus irbesartan in patients with chronic kidney disease, United Kingdom Heart and Renal Protection (HARP)-III–rationale, trial design and baseline data, Nephrol Dialysis Transp. 32 (12) (2016) 2043–2051, doi:10.1093/ndt/gfw321.

[17] M. Packer, Leptin-aldosterone-neprilysin axis, identification of its distinctive role in the pathogenesis of the three phenotypes of heart failure in people with obesity, Circulation 137 (15) (2018) 1614–1631, doi:10.1161/CIRCULATIONAHA.117.032474.

[18] N. Esser, S. Zraika, Neprilysin inhibition: a new therapeutic option for type 2 diabetes? Diabetologia (2019) 1–10, doi:10.1007/s00125-019-4889-y.

[19] D.A. Aykan, T.T. Koca, S. Yaman, N. Eser, Angiotensin converting enzyme and neprilysin inhibition alter pain response in dexamethasone-induced hypertensive rats, Pharmacol. Rep. 71 (2) (2019) 306–310, doi:10.1016/j.pharep.2018.12.002.

[20] K. Yang, C. Zhang, L. Sun, D. Li, X. Hong, Cigarette smoke condensate could promote human bronchial epithelial BEAS-2B cell migration through shifting neprilysin trafficking, J. Cancer Res. Therap. 14 (10) (2018) 680, doi:10.4103/0973-1482.183182.

[21] J. Turečková, M. Vojtěchová, M. Krausová, E. Šloncová, V. Korínek, Focal adhesion kinase functions as an akt downstream target in migration of colorectal cancer cells, Transl. Oncol. 2 (4) (2009) 281–290, doi:10.1593/tlo.09160.

[22] D. Acanfora, M.M. Ciccone, P. Scicchitano, C. Acanfora, G. Casucci, Neprilysin inhibitor–angiotensin II receptor blocker combination (sacubitril/valsartan): rationale for adoption in SARS-CoV-2 patients, Eur. Heart J.—Cardiovascular Pharmacothe. (2020), doi:10.1093/ehjcvp/pvaa028.

[23] D. Acanfora, M.M. Ciccone, P. Scicchitano, C. Acanfora, G. Casucci, Sacubitril/valsartan in COVID-19 patients: the need for trials, Eur. Heart J.—Cardiovasc. Pharmacothe. (2020), doi:10.1093/ehjcvp/pvaa044.

[24] T.-D. Wang, Renin-angiotensin system inhibitors and COVID-19: potential therapeutics rather than perpetrators, Acta Cardiologica Sinica 36 (3) (2020) 179, doi:10.6515/ACS.202005_36(3).20200430A.

[25] K. Park, A review of computational drug repurposing, Transl. Clinic. Pharmacol. 27 (2) (2019) 59–63, doi:10.12793/tcp.2019.27.2.59.

[26] S. Kumar, S. Chowdhury, S. Kumar, In silico repurposing of antipsychotic drugs for Alzheimer's disease, BMC neuroscience 18 (1) (2017) 76, doi:10.1186/s12868-017-0394-8.

[27] N. Schiering, A. D'Arcy, F. Villard, P. Ramage, C. Logel, F. Cumin, G.M. Ksander, C. Wiesmann, R.G. Karki, M. Mogi, Structure of neprilysin in complex with the active metabolite of sacubitril, Sci. Rep. 6 (2016) 27909, doi:10.1038/srep27909.

[28] G.M. Sastry, M. Adzhigirey, T. Day, R. Annabhimoju, W. Sherman, Protein and ligand preparation: parameters, protocols, and influence on virtual screening enrichments, J. Comput. Aided Mol. Des. 27 (3) (2013) 221–234, doi:10.1007/s10822-013-9644-8.

[29] A. Kumar, E. Rathi, S.G. Kini, E-pharmacophore modelling, virtual screening, molecular dynamics simulations and in-silico ADME analysis for identification of potential E6 inhibitors against cervical cancer, J. Mol. Struct. 1189 (2019) 299–306, doi:10.1016/j.molstruc.2019.04.023.

[30] J. Irwin, T. Sterling, T. Mysinger, MM Bolstad, ES Coleman, RGJ Chem. Inf. Model. 52 (2012) 1757.

[31] I. Nagpal, I. Raj, N. Subbarao, S. Gourinath, Virtual screening, identification and in vitro testing of novel inhibitors of O-acetyl-L-serine sulfhydrylase of Entamoeba histolytica, PLoS One 7 (2) (2012) e30305, doi:10.1371/journal.pone.0030305.

[32] A. Kumar, E. Rathi, S.G. Kini, Drug repurposing approach for the identification and designing of potential E6 inhibitors against cervical cancer: an in silico investigation, Struct. Chem. (2019) 1–13.

[33] E. Rathi, A. Kumar, S.G. Kini, Molecular dynamics guided insight, binding free energy calculations and pharmacophore-based virtual screening for the identification of potential VEGFR2 inhibitors, J. Recept. Signal Transduct. (2019) 1–19, doi:10.1080/10799893.2019.1690509.

[34] S.B. Mallik, A. Pai, R.R. Shenoy, B. Jayashree, Novel flavonol analogues as potential inhibitors of JMJD3 histone demethylase—A study based on molecular modelling, J. Mol. Graph. Model. 72 (2017) 81–87, doi:10.1016/j.jmgm.2016.12.002.

[35] A.L. Bowman, Z. Nikolovska-Coleska, H. Zhong, S. Wang, H.A. Carlson, Small molecule inhibitors of the MDM2-p53 interaction discovered by ensemble-based receptor models, J. Am. Chem. Soc. 129 (42) (2007) 12809–12814, doi:10.1021/ja073687x.

[36] A. Hospital, J.R. Goñi, M. Orozco, J.L. Gelpí, Molecular dynamics simulations: advances and applications, Adv. Appli. Bioinform. Chem.: AABC 8 (2015) 37, doi:10.2147/AABC.S70333.

[37] L.M. Lima, E.J. Barreiro, Bioisosterism: a useful strategy for molecular modification and drug design, Curr. Med. Chem. 12 (1) (2005) 23–49, doi:10.2174/0929867053363540.

[38] C. Oefner, A. D'Arcy, M. Hennig, F.K. Winkler, G.E. Dale, Structure of human neutral endopeptidase (Neprilysin) complexed with phosphoramidon, J. Mol. Biol. 296 (2) (2000) 341–349, doi:10.1006/jmbi.1999.3492.

[39] S. Voisin, D. Rognan, C. Gros, T. Ouimet, A three-dimensional model of the neprilysin 2 active site based on the X-ray structure of neprilysin identification of residues involved in substrate hydrolysis and inhibitor binding of neprilysin 2, J. Biol. Chem. 279 (44) (2004) 46172–46181, doi:10.1074/jbc.m407333200.

[40] A.J. Turner, Neprilysin, in: Handbook of proteolytic enzymes, Elsevier, 2004, pp. 419–426.

[41] N.C.f.B.I. National Library of Medicine, https://pubchem.ncbi.nlm.nih.gov/compound/Indomethacin, 2020. (Accessed 09/08/2020 2020).

[42] N.C.f.B.I. National Library of Medicine, https://pubchem.ncbi.nlm.nih.gov/compound/Tyropanic-acid, 2020. (Accessed 09/08/2020 2020).

[43] Swiss Institute of Bioinformatics, http://www.swissadme.ch/, 2020. (Accessed 10/08/2020 2020).

[44] H.A. Zhong, in: ADMET properties: Overview and current topics, Drug Design: Principles and Applications, Springer, 2017, pp. 113–133, doi:10.1007/978-981-10-5187-6_8.

[45] A. Tornio, J.T. Backman, Cytochrome P450 in pharmacogenetics: an update, in: Advances in Pharmacology, Elsevier, 2018, pp. 3–32, doi:10.1016/bs.apha.2018.04.007.

[46] U.M. Zanger, M. Schwab, Cytochrome P450 enzymes in drug metabolism: regulation of gene expression, enzyme activities, and impact of genetic variation, Pharmacol. Ther. 138 (1) (2013) 103–141, doi:10.1016/j.pharmthera.2012.12.007.